Pseudohalide Functional additive in Tin Halide Perovskite for Efficient and Stable Pb-free Perovskite Solar Cells

Dhruba B. Khadka†*, Yasuhiro Shirai†, Masatoshi Yanagida† and Kenjiro Miyano†

†Photovoltaic Materials Group, Center for GREEN Research on Energy and Environmental Materials, National Institute for Materials Science (NIMS), 1-1 Namiki, Tsukuba, Ibaraki 305-0044, Japan

Corresponding Author
*E-mail: KHADKA.B.Dhruba@nims.go.jp

ABSTRACT

The progress of tin-based halide perovskite solar cells (Sn-HaPSCs) is obstructed by their poor stability arising from tin oxidation. Herein, we introduced the phenethylammonium thiocyanate (PEASCN) as a pseudohalide functional additive into $FASnI_3$ perovskite film to improve the optoelectronic properties. This approach is found to be effective for the suppression of Sn-oxidation and the formation of compact and larger grain film with a higher degree of crystallinity. The device with PEASCN additive improved the device efficiency from 4.52% (for pristine Sn-HaP) to 9.65% with a significant increase of V_{OC} from ~0.411 to 0.667 V and superior device stability. The device analysis revealed that the PEASCN additive has improved the optoelectronic properties coupled with a higher diffusion potential and suppression of bulk and interface defect in the Sn-HaPSC. This work corroborates that the incorporation of pseudohalide-based functional additive in the $FASnI_3$ is propitious for better film formation, passivation of detrimental surface chemistry, and defects at interface and bulk.

Keywords: Tin perovskite, lead free, tin oxidation, device stability, pseudohalide, defect profile

1. Introduction

Tin halide perovskite solar cells (Sn-HaPSCs) have gained attention as an alternative to lead-based halide perovskite devices to solve the toxicity issue of lead.[1] Albeit Sn-perovskite exhibits promising optoelectrical properties such as high absorption coefficients, small exciton binding energy, and high carrier mobilities,[2] its intrinsic instability due to the facile oxidation of Sn^{2+} to Sn^{4+} leads to the formation of tin vacancy and metal-like behavior that deteriorates the device performance.[3] Indeed, tin has a weakly bonded pair ($5s^2$) that results in the Sn^{2+}/Sn^{4+} oxidation spontaneously. It endorses self-p-doping in the Sn-HaP film leading to shorting of the device[4] and exacerbates the non-radiative recombination dynamics.[5]

Several approaches have been introduced that passivate the catastrophic effects in Sn-HaP film quality by structural regulation and additive engineering which results in improving the device performance and its stability.[6] The additives such as tin(II) halide,[7] Sn-powder,[8] hydrazine derivatives,[9,10] thiosemicarbazide,[11] fluoro-aniline isomers,[12] and pyrazine[13] have been used as reducing agents to inhibit the oxidation and facilitate the formation of a pinhole-free uniform film. Similarly, the incorporation of co-cations[14,15] and mixed anions[16,17] in formamidinium tin tri-iodide ($FASnI_3$) play a prominent role to control the film morphology and reduce the oxidation resulting in better power conversion efficiency (PCE). The A-site cations such as methylammonium (MA),[3] guanidinium (GA),[14] Cs,[18] and Rb[15] mixed with $FASnI_3$ have demonstrated improvement in the device performance and stability by regulating 3D structure. Moreover, introducing bulky hydrophobic ammonium cation derivatives such as butylammonium (BA^+),[19] phenylethylammonium (PEA^+),[20,21] 5-ammonium valeric acid (5-AVA),[22] ethylenediammonium (EDA)[14] in $FASnI_3$ give 3D/2D composite. Adopting this approach, Hayase and co-workers[23] reported PCE over 13% using Sn-HaP absorber layer with mixed cations and GeI_2. Besides this, a thin 2D layer was formed on the top of the 3D layer by post-treatment using such as PEABr/IPA[24] or 4-(trifluoromethyl)benzyl ammonium/chloroform.[25] Diau and co-workers[26] have reported 3D/2D structured devices using a number of bulky ammonium cations (e.g. hexylammonium, cyclohexylammonium, anilinium, etc)/hexafluoro-2-propanol treatment with promising efficiency and great stability in ambient air. A recent report demonstrated a record efficiency as high as 14.6% using $SnI_2.(DMSO)_x$ adduct coupled along with PEABr additive.[27] A theoretical study[28] on the chemistry of Sn suggested that the Sn-X bond in tin halide is more vulnerable to water and oxygen which is prone to poor device stability. Several reports demonstrated that the additives with pseudohalide functional derivatives increase the device performance of HaPSCs and stability coupled with the hydrophobicity and optoelectronic quality of HaP film.[29–32] Polyatomic

pseudohalide such as thiocyanate (SCN^-), azide (N_3^-), tetrahydroborate (BH_4^-), formate ($HCOO^-$), and methanethiolate (CH_3S^-) have been studied as a candidate for the X-site tailoring.[33,34] It is documented that the additive with N-, S-, and O- based electron donors can conjugate with tin halides by donating a lone pair electron to the divalent tin resulting increase in covalency.[35,36] Albeit the introduction of pseudohalide is propitious for stabilizing the halide bonding,[37–39] only a handful of works have been carried out for Sn-based HaPSCs. The pseudohalide $SCN^-$of GA[40] and FA[16,41] as an additive in $FASnI_3$ resulted in improvement in device performance. It is documented that π-conjugated electronic system of the pseudohalide SCN^-coordinates with Sn^{2+} ion and controls the extent of oxidation in Sn-based film.[16,42] The functional additives with thiocyanate anion are also beneficial for film growth,[43,44] moisture tolerance,[45] and carrier transport.[46,47] Accounting for these beneficial aspects, it is worthwhile to explore the functional additive to understand the effect of pseudohalide in Sn-HaPSCs.

Herein, we introduced the bulky organic cation pseudohalide PEASCN in the $FASnI_3$ precursor to control the extent of tin oxidation and film growth for the development of Sn-HaPSCs. It is found that the pseudohalide of the PEASCN additive effectively improves the film quality and optoelectronic properties. The device efficiency improved from 4.52% for pristine to 9.65% for additive with higher reproducibility and improved stability. The film and device analysis revealed that the PEASCN additive catalyses the growth of large grains with highly oriented crystalline orientation, longer carrier lifetime, and defect passivation. We have underscored the insight into a pseudohalide additive approach to pave the way for resolving the oxidation and deterioration issue of Sn-HaPSCs.

2. Results and discussion

The $FASnI_3$ films were prepared with different additive ratios of PEASCN by one-step fast deposition subsequent with an antisolvent dripping approach as described in the experimental section. XRD measurements were carried out to study the impacts of PEASCN additive on the Sn-HaP films. All the XRD patterns (Fig.1a) showed characteristic diffraction peaks consistent with the orthorhombic phase of $FASnI_3$.[7,48] We observed highly oriented crystallographic planes of (100) and (200) for Sn-HaP films with PEASCN additive whereas the pristine film grows with multiple crystal orientations i.e. (102), (122), (222), (213), etc. As the XRD results in the small-angle regime (Fig. 1a, left) show an additional diffraction peak for $x \geq 0.12$ suggesting the formation of a 2D layer with phenethylammonium cation.[19,20,49] No 2D layer features were observed with PEASCN additive for $x \leq 0.08$. Moreover, one can see an asymmetric characteristic peak for the pristine film compared to those films with PEASCN

additive (Fig. 1a, right). The asymmetric characteristic feature is attributed to the poor crystalline nature. Although the shifting of characteristic peaks is hardly observed, we can eye a slight incline in diffraction angle suggesting incorporation of SCN^- molecular ions into the crystal lattice. A similar observation has been reported with the introduction of phenylhydrazine hydrochloride[48] and with the addition of SCN functional derivatives.[16] It has been documented that PEA^+ has a large ionic radius that does not fit into the corner-sharing $[PbI_6]^{4-}$and it separate 3D HaP into layer rather than incorporation in crystal lattice.[50] Since the ionic radius of I^-(2.20 nm) is similar to that of SCN^-(2.15-2.20 nm), it does not induce a significant change in lattice with the incorporation of SCN^-.[42] However, the ambident nucleophilic nature of SCN^-acts as a bridging ligand to form a stable 3D network of octahedral. This characteristic feature of pseudohalide functional additive results in the growth of the high-quality crystalline film.

The absorption spectra of the films (x=0-0.12) (Figure 1b) demonstrate some effects with a higher content of PEASCN additive. A distinct absorption curve for x=0.12 might be a consequence of the formation of a 2D layer of PEA_2SnI_4 (as seen in XRD pattern; Fig. 1a) with higher content of PEA^+ in the film that affects a band edge. Photoluminescence (PL) spectra of the corresponding films (Fig. 1c) display a slight blueshift with the introduction of PEASCN. The characteristic PL peaks are centred at 1.40 ± 0.02 eV for x=0 and 1.46 ± 0.02 eV for x=0.12. It is noticed that the PL spectra with $0<x<0.12$ are comparatively symmetric that could be related to the improvement in optoelectronic quality.

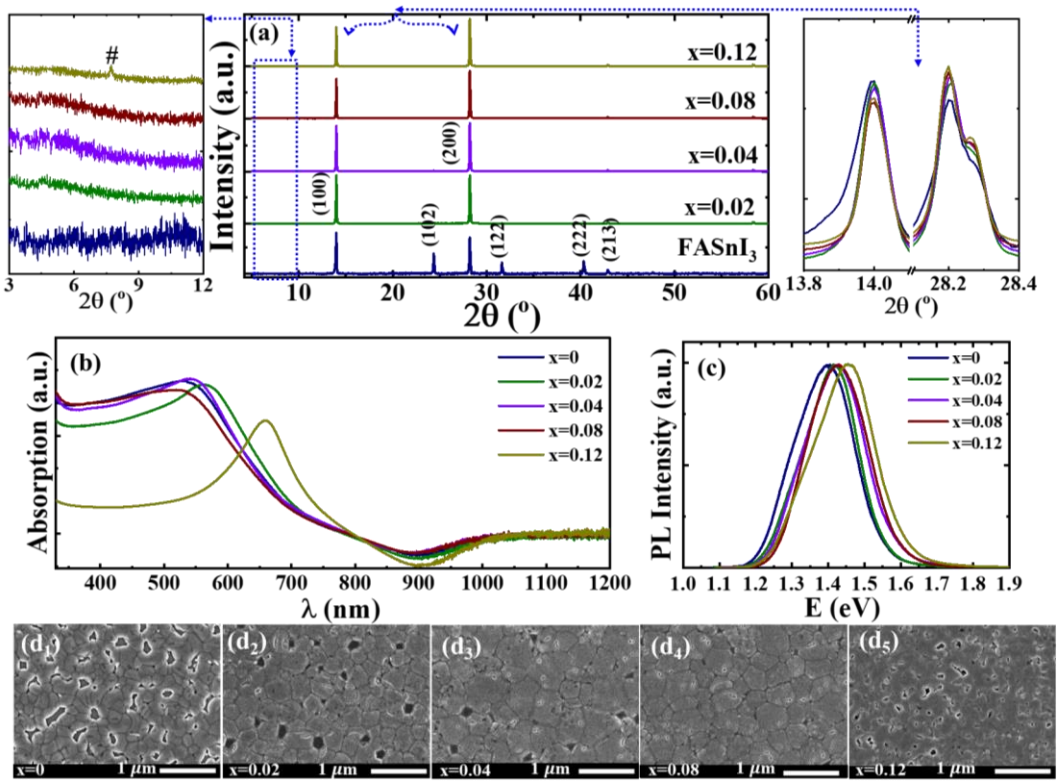

Fig. 1 Growth characteristics of the $FASnI_3$ films with different amount of PEASCN additive (x=0-0.12) with respect to FAI. (a) XRD patterns (left- small angle- XRD pattern; 2θ<10, right- zoomed-in XRD patterns with dominant peaks (100) and (200)), (b) absorption spectra, (c) PL spectra, and (d_1-d_5) SEM images of pristine (x=0) and film with additives. # - corresponds to characteristics peak for 2D layer of PEA_2SnI_4.

Figure 1d_1-d_5 shows the top view scanning electron microscopic (SEM) images of the corresponding films. The pristine $FASnI_3$ film shows a very poor film coverage with numerous pinholes which is deleterious for shunting path in the device. The films with PEASCN additive exhibit a significant improvement in film coverage by suppressing the pinhole's densities. However, the film with a higher PEASCN additive (x>0.08) was found to be grown with uneven morphology. This could be due to the uneven formation of 2D layered features at the surface of the film in the nanoscale range.[20,49] Moreover, the average grain sizes are in the range of ~50- 300 nm for the pristine film while those for the films with PEASCN additives are ~150-600 nm. These improvements in film growth with the addition of PEASCN may be due to the collective effect. It has been documented that the rapid crystal growth of pristine $FASnI_3$ leads to the pinhole rich morphology that can be slowed down by functional additive engineering (i.e. adding the bulky organic cations with iodine such as PEAI, GAI, or $EDAI_2$).[14,20] It is also observed that the pseudohalide functional additive promotes film growth and enhances optoelectronic properties.[16,34,38,40,42] With the favor of documented growth

mechanism, it is believed that the PEA^+ plays a crucial role in deaccelerate the crystal growth by extended bonding interaction. On the other hand, the pseudohalide anion (SCN^-) also facilitates the coarsening of grains and improves the film quality.

We then fabricated a complete device with the inverted structure of ITO/PEDOT:PSS/Sn-HaP/PCBM/BCP/Ag as depicted in the cross-sectional image (Fig. 2a). Figure 2b shows the current density-voltage (*J-V*) curves of pristine and the best device with PEASCN additive. The device parameters with different additive contents are summarized in Table 1 and corresponding *J-V* curves are given in Fig. S1a. The device with pristine $FASnI_3$ achieved a *PCE* of 4.52% (with J_{SC}~19.76 mA/cm^2, V_{OC}~0.411V, and FF~55.6%). The *J-V* characteristic (Fig. 2b) with PEASCN additive ($x \leq 0.08$) in $FASnI_3$ (hereafter, $FASnI_3$ with PEASCN additive) demonstrated an improved device performance of 9.65% with significantly improved in V_{OC}~ 0.667 V and *FF*~65.3%, and J_{SC}~22.15 mA/cm^2 (steady-state J_{SC} and *PCE*; Fig. S2) This is attributed to the growth of compact and large grain morphology with high crystal quality leading to the betterment in optoelectronic properties. However, the device with a higher additive gives a lower performance which is related to the poor film morphology caused by uneven surface and worsened optophysical properties as indicated by asymmetric features (Fig.1c, d). In addition, the statistical data (Fig. 2c and Fig. S3) show a narrower distribution of device parameters for the device with PEASCN additive indicating higher reproducibility compared to the device with pristine $FASnI_3$.

Figure 2d displays the external quantum efficiency (*EQE*) of the device with pristine $FASnI_3$ and with PEASCN additives (Fig. S1b). It shows a noticeable enhancement in the 350-850 nm regime suggesting the improved interface and absorber quality with PEASCN additives.[51] . The values of J_{SC} estimated by integrating the *EQE* spectra are 19.54 and 21.76 mA/cm^2 for the corresponding devices. These values are slightly lower but in the range of the value obtained from the *J–V* curves (Fig. 2b). The band edges estimated from *EQE* spectra (inset, Fig. 2d) reveals a little blue shift for the device with PEASCN additive. This is consistent with the absorption and PL characteristics (Fig. S4 and Fig. 1b,c).

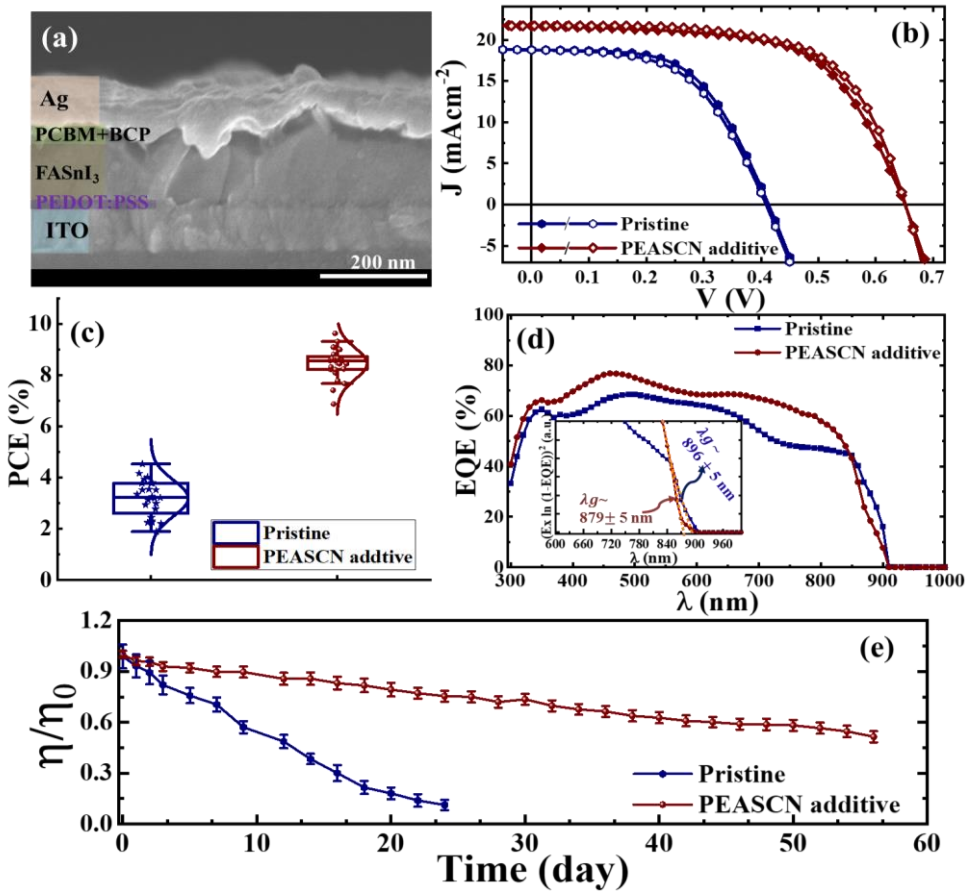

Fig. 2. Cross-sectional image of the device (a), *J-V* curves of $FASnI_3$ devices (pristine and PEASCN additive (0.08 mol%) (■ forward/□ reverse scan direction) (b), statistics of *PCE* (η) (c), *EQE* spectra (d), and stability of encapsulated device (e).

Table 1. The device parameters of the $FA_{1-x}PEA_xSnI_3$ devices with different PEASCN content (x=0-0.12). The best device parameters are given outside the parentheses. The average values PCE and standard deviation (40 devices from 4 batches) are given in parentheses.

$FASnI_3$+PEASCN (FAI:PEASCN=1-x:x)	0	0.02	0.04	0.08	0.12
Jsc (mA/cm^2)	19.76	19.85	21.45	22.16	14.48
Voc (V)	0.411	0.479	0.543	0.667	0.517
FF	0.556	0.595	0.623	0.653	0.523
Rs ($\Omega \cdot cm^2$)	5.46	5.32	4.32	3.35	6.10
Rsh ($k\Omega \cdot cm^2$)	0.872	0.978	0.959	2.570	0.846
η (%)	4.52 (3.52±0.58)	5.66 (4.82±0.62)	7.26 (6.72±0.46)	9.65 (8.92±0.27)	3.92 (3.26±0.74)

The device performance monitored with time (Fig. 2e and Fig. S5) demonstrates that the device with PEASCN additive has superior device stability. The XRD results (Fig. S6) revealed that the pristine $FASnI_3$ deteriorates stemming from a dominant SnI_2 secondary peak, whereas the film with PEASCN additive is comparatively stable retaining characteristics with few obscure peaks. These results agree with the other's reports which have used pseudohalide functional additive for tailoring the absorber layer properties.[16,52] Thus, these results suggest that the PEASCN additive in the $FASnI_3$ absorber is advantageous for the improvement in device performance as well as device stability. Comparing with Pb-based devices, the PCE and device stability are still impeded due to the Sn-HaP film quality. Therefore, it is imperative to resolve the impedance factors for getting competitive device quality.

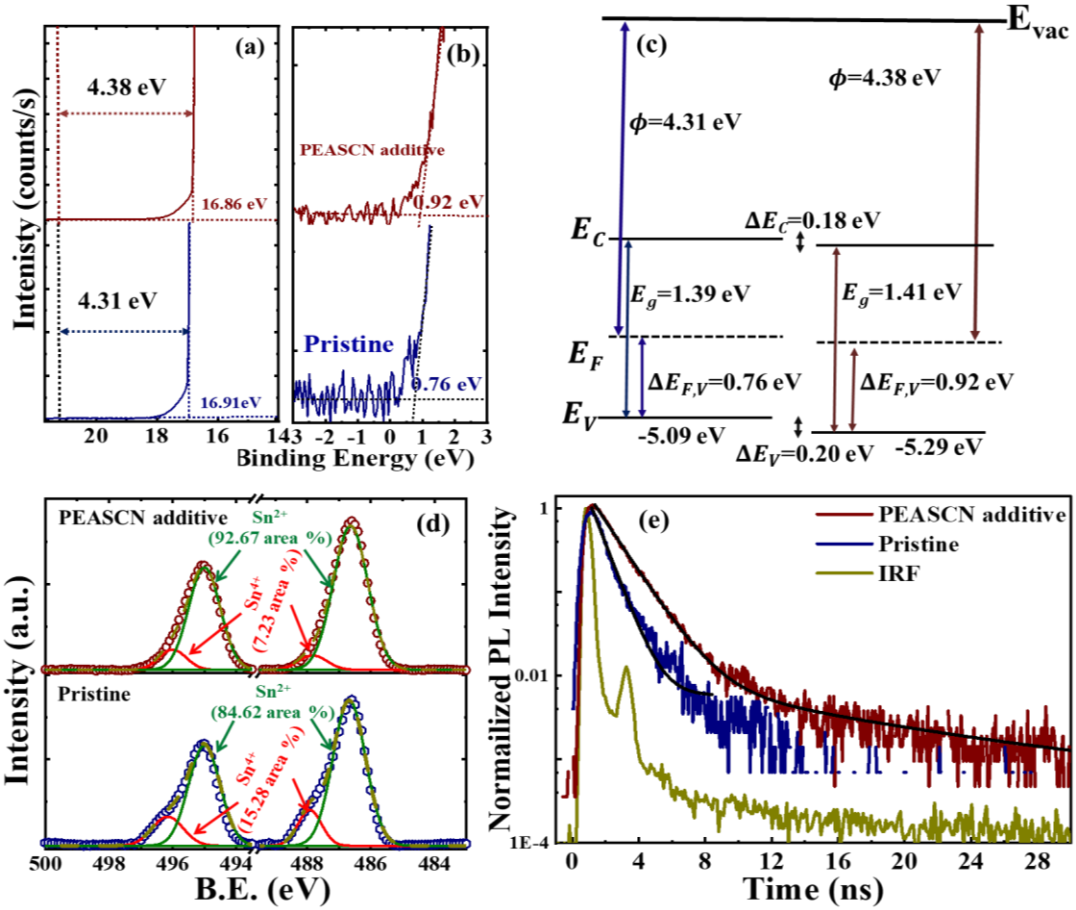

Fig. 3. UPS spectra of the $FASnI_3$ films of pristine and with PEASCN additive; (a) the photoemission cutoff energy and (b) valence band spectra with the energy difference between the valence band maximum (E_V) and the Fermi level (E_F). (c) schematic illustration of energy levels. (d) XPS-spectra (Sn 3d: $3d_{5/2}$ and $3d_{3/2}$) of the surface of the $FASnI_3$ films without and with PEASCN addition. (e) TRPL decay spectra for corresponding films.

To understand the impact on energy band, we characterized the $FASnI_3$ film without and with PEASCN additive using ultraviolet photoelectron spectroscopy (UPS). The work function

(ϕ) (Fig. 3a) and the difference between the valence band and Fermi level ($\Delta E_{F,V}$=E_V-E_F) (Fig. 3b) indicate a slight increase value for the $FASnI_3$ film with PEASCN additive. We calculated band structure (Fig. 3c, energy band diagram, Fig. S7) by combining optical bandgap (Fig. 1c and 2d). It reveals that an increase in work function with a downshift of E_V and E_C level reduces the band offset which benefits the effective carrier transfer and increases the V_{OC} as well as other device parameters.[21] It is concurrent with our device results.

To explore the surface chemistry, the film was studied by X-ray photoelectron spectroscopy (XPS) (Fig. S8). The two characteristic peaks deconvoluted into the Sn 3d ($3d_{5/2}$ ($3d_{3/2}$)) (Fig. 3d) at ~486.7 (495.2) eV and 487.3 (495.7) eV are attributed to the Sn^{2+} and Sn^{4+} species, respectively. Moreover, the surface composition extracted from the XPS spectra (Tables ST1 and ST2) shows iodine poor composition (*i.e.* an atomic ratio of Sn : I of 1 : 1.38 for the pristine and 1 : 1.69 for the PEASCN additive) for both films. Accounting for the detection limit of XPS (<10 nm), the off-stoichiometric film surface could be related to the existence of a higher content of SnF_2 or iodine loss due to surface oxidation. The analysis of Sn 3d core spectra demonstrated that the atomic percentage of Sn^{4+} for the film with PEASCN additive is suppressed from 15.28 to 7.23% (Fig. 3d). A comparative analysis of XPS spectra of C, N, and S (Fig. S9) suggests that SCN^- pseudohalide interacts with Sn^{2+} that increases the bonding strength against facile oxidation.[42] Moreover, the pseudohalide anion has a higher binding affinity that passivates iodine vacancies present at the surface or grain boundaries of the Sn-HaP.[34] Hence the PEASCN additive improves the stability of the $FASnI_3$ film. Thus, it corroborates that the ionic species of additive; PEA^+/SCN^- coordinate with Sn^{2+} ion and mitigates the formation of notorious species (Sn^{4+}, I_2) on the film surface and bulk. And hence, it controls the extent of oxidation in the Sn-based film.

Figure 3e shows time-resolved PL (TRPL) characteristics of Sn-HaP film prepared on the glass substrate. The PL lifetime shows a longer carrier lifetime of 1.68 ns for the PEASCN added $FASnI_3$ film compared to the pristine film (0.64 ns). A similar value of lifetime has been reported for $FASnI_3$ film with functional additives.[14,36] This indicates a lower defect density in the film with an additive that must be a consequence of the controlled growth of morphology with large grain and better crystallinity of film with additive. However, the PL lifetime of the $FASnI_3$ film is much lower than the Pb-HaP film.[53] This could be the result of a dominant effect of the metallic nature of Sn^{4+} existed in the Sn-HaP film.

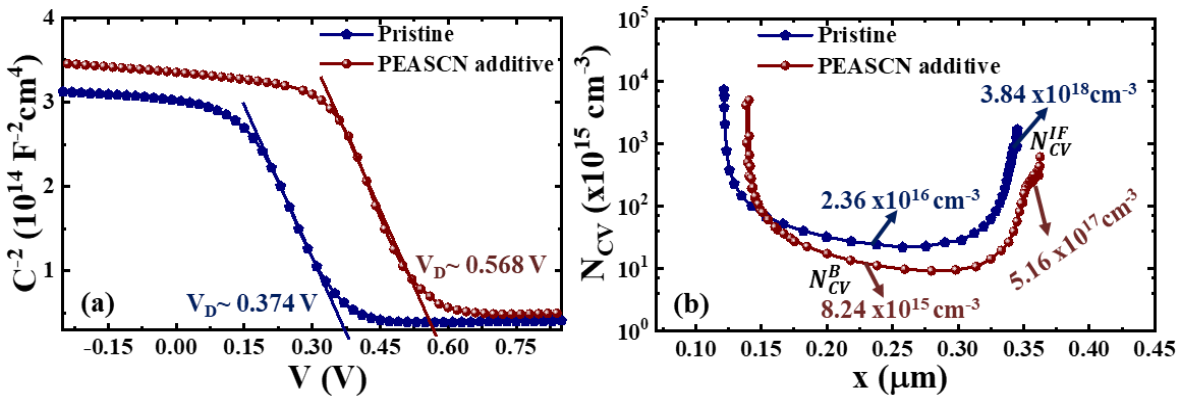

Fig. 4. Capacitance-voltage (*C-V*) characteristics of devices; (a) Mott-Schottky plots and (b) carrier profile extracted from *C-V* analysis.

To get insight into the defect densities, we further studied the capacitance characteristics of the device to study the impact of additives on the carrier profile. The capacitance response accounts for the carrier distribution (free carrier and defect density)[54,55] and ion or charge accumulation at the interface[56] in thin-film solar cells. The capacitance-frequency (*C-f*) response (Fig. S10) for the pristine device shows a slightly larger value in the range of 1kHz to 50 kHz that stems from the absorber layer. It implicates a higher defect density in the pristine Sn-HaP film which is prone to inferior device performance. Similarly, the capacitance at a lower frequency which accounts for the ionic motion or charge accumulation,[56,57] has a lower value for the device with PEASCN additive. It is attributed to the reduction in ion or charge accumulation at the interfacial layer or electrode that could be propitious for device stability (Fig. 2e). To have a quantitative analysis carrier and defect profile, we measured capacitance-voltage (*C-V*) response and analyzed the Mott-Schottky (M-S) curves (Eq. 1) and carrier profile (Eqn.2) given by the relation.[58]

$$\left(\frac{1}{C(V)}\right)^2 = \frac{2}{q\varepsilon_0\varepsilon_s N_A(x)}(V + V_D) \qquad (1)$$

$$N_{CV} = -\frac{2}{q\varepsilon_0\varepsilon_s}\left[\frac{d}{dV}\left(\frac{1}{C(V)^2}\right)\right]^{-1} \qquad (2)$$

where C - capacitance per area, ε_0-permittivity of free space, ε_s - a dielectric constant of perovskite layer which is estimated from the plateau region of *C-f* plot measured at zero bias under dark. V_D denotes a diffusion potential, (defined by $V_D = V_{bi} - E_F/q$; where Fermi energy- E_F and built-in potential- V_{bi}). N_{CV} represents the carrier distribution profile corresponding to calculated from C-V curves.

Figure 4a displays the *M-S* plots of respective devices. It demonstrates an increase in diffusion potential (V_D)[58] from 0.374 to 0.568 V for the device with PEASCN additive, which

is parallel to the increase in the V_{OC}. Figure 4b gives the wide U-shaped carrier profile estimated from *C-V* spectra. According to our calculation by *C-V* analysis, the $FASnI_3$ film has a bulk carrier density (N_{CV}^{B}) of ~2.36×10^{16} cm^{-3} that has reduced to ~8.24×10^{15} cm^{-3} for the film with PEASCN additive. Similarly, the edge of carrier profile accounts for the interface defect profile (N_{CV}^{IF} ~3.84×10^{18} for pristine to ~$5.16\times10^{17}cm^{-3}$ for the PEASCN additive) are reduced by approximately on order for the device with PEASCN. A lower carrier density is attributed to less Sn^{4+} densities and hence attenuated recombination in the device. Thus, the N_{CV} results corroborate that the PEASCN additive mitigates the bulk defect at the space charge region or intrinsic regime as well as interface defect profile. And hence it contributes to improving the device parameters. A similar result was reported by Diau and co-workers showing a reduction of carrier density in the device with pristine $FASnI_3$ (7.2×10^{16} cm^{-3}) by a few fractions in magnitude with butylammonium iodide as a functional additive (6.2×10^{16} cm^{-3}).[19] Lee et al. have also documented the carrier density suppressed by 3 orders of magnitude for a Br-doped $FASnI_3$ device (6.76×10^{17} to 7.80×10^{14} cm^{-3}).[17] These reports collectively implicate that the functional additive, as well as compositional engineering, are beneficial for defect passivation. the N_{CV} profile also supports a longer carrier lifetime given by TRPL results (Fig. 3e) as well as the reduction of the extent of oxidation of Sn^{2+} as observed in the XPS analysis (Fig.3d). Thus, it is believed that the organic cation (PEA^{+}) as well as pseudo halide (SCN^{-}) play a vital role to improve optoelectronic properties of the Sn-HaP absorber layer. Our work suggests that the functional additives with pseudohalide anion derivatives could open a new door for further improvement in device performance and stability.

3. Conclusions

We fabricated Sn-HaPSCs of efficiency ~9.65% using phenethylammonium thiocyanate (PEASCN) additive with superior stability. The $FASnI_3$ film with the pseudohalide functional additive not only remarkably improved the film morphology and highly oriented crystal growth but also inhibited Sn^{2+}/Sn^{4+} oxidation. We found that the $FASnI_3$ film with additive increases the carrier lifetime and reduces the band offset. From capacitance analysis, the diffusion potential (0.374 V for pristine) was found to be increased to 0.568 V for the device with PEASCN additive with the suppression of defect densities in the bulk and at the interface. Our report substantiates that the pseudohalide functional is expedient for the improvement of film morphology and optoelectronic quality of $FASnI_3$ film that hikes the performance as well as stability of Sn-HaPSCs.

Supporting Information

The Supporting Information is available on the website.

Acknowledgements

This work was financially supported the Yazaki Foundation.

Conflicts of interest

There are no conflicts to declare.

References

(1) Nasti, G.; Abate, A. Tin Halide Perovskite (ASnX3) Solar Cells: A Comprehensive Guide toward the Highest Power Conversion Efficiency. *Adv. Energy Mater.* **2020**, *10* (13), 1902467. https://doi.org/10.1002/aenm.201902467.

(2) Baranowski, M.; Plochocka, P. Excitons in Metal-Halide Perovskites. *Adv. Energy Mater.* **2020**, *10* (26), 1903659. https://doi.org/10.1002/aenm.201903659.

(3) Nakamura, T.; Yakumaru, S.; Truong, M. A.; Kim, K.; Liu, J.; Hu, S.; Otsuka, K.; Hashimoto, R.; Murdey, R.; Sasamori, T.; Kim, H. Do; Ohkita, H.; Handa, T.; Kanemitsu, Y.; Wakamiya, A. Sn(IV)-Free Tin Perovskite Films Realized by in Situ Sn(0) Nanoparticle Treatment of the Precursor Solution. *Nat. Commun.* **2020**, *11* (1), 3008. https://doi.org/10.1038/s41467-020-16726-3.

(4) Hao, F.; Stoumpos, C. C.; Guo, P.; Zhou, N.; Marks, T. J.; Chang, R. P. H.; Kanatzidis, M. G. Solvent-Mediated Crystallization of CH3NH3SnI3 Films for Heterojunction Depleted Perovskite Solar Cells. *J. Am. Chem. Soc.* **2015**, *137* (35), 11445–11452. https://doi.org/10.1021/jacs.5b06658.

(5) Kamarudin, M. A.; Hirotani, D.; Wang, Z.; Hamada, K.; Nishimura, K.; Shen, Q.; Toyoda, T.; Iikubo, S.; Minemoto, T.; Yoshino, K.; Hayase, S. Suppression of Charge Carrier Recombination in Lead-Free Tin Halide Perovskite via Lewis Base Post-Treatment. *J. Phys. Chem. Lett.* **2019**, *10* (17), 5277–5283. https://doi.org/10.1021/acs.jpclett.9b02024.

(6) Yan, Y.; Pullerits, T.; Zheng, K.; Liang, Z. Advancing Tin Halide Perovskites: Strategies toward the ASnX3 Paradigm for Efficient and Durable Optoelectronics. *ACS Energy Lett.* **2020**, *5* (6), 2052–2086. https://doi.org/10.1021/acsenergylett.0c00577.

(7) Liao, W.; Zhao, D.; Yu, Y.; Grice, C. R.; Wang, C.; Cimaroli, A. J.; Schulz, P.; Meng, W.; Zhu, K.; Xiong, R.-G.; Yan, Y. Lead-Free Inverted Planar Formamidinium Tin

Triiodide Perovskite Solar Cells Achieving Power Conversion Efficiencies up to 6.22%. *Adv. Mater.* **2016**, *28* (42), 9333–9340. https://doi.org/10.1002/adma.201602992.

(8) Lin, R.; Xiao, K.; Qin, Z.; Han, Q.; Zhang, C.; Wei, M.; Saidaminov, M. I.; Gao, Y.; Xu, J.; Xiao, M.; Li, A.; Zhu, J.; Sargent, E. H.; Tan, H. Monolithic All-Perovskite Tandem Solar Cells with 24.8% Efficiency Exploiting Comproportionation to Suppress Sn(Ii) Oxidation in Precursor Ink. *Nat. Energy* **2019**, *4* (10), 864–873. https://doi.org/10.1038/s41560-019-0466-3.

(9) Tsarev, S.; Boldyreva, A. G.; Luchkin, S. Y.; Elshobaki, M.; Afanasov, M. I.; Stevenson, K. J.; Troshin, P. A. Hydrazinium-Assisted Stabilisation of Methylammonium Tin Iodide for Lead-Free Perovskite Solar Cells. *J. Mater. Chem. A* **2018**, *6* (43), 21389–21395. https://doi.org/10.1039/C8TA07699E.

(10) Wang, C.; Zhang, Y.; Gu, F.; Zhao, Z.; Li, H.; Jiang, H.; Bian, Z.; Liu, Z. Illumination Durability and High-Efficiency Sn-Based Perovskite Solar Cell under Coordinated Control of Phenylhydrazine and Halogen Ions. *Matter* **2021**, *4* (2). https://doi.org/10.1016/j.matt.2020.11.012.

(11) Li, B.; Di, H.; Chang, B.; Yin, R.; Fu, L.; Zhang, Y.-N.; Yin, L. Efficient Passivation Strategy on Sn Related Defects for High Performance All-Inorganic CsSnI3 Perovskite Solar Cells. *Adv. Funct. Mater.* **2021**, *31* (11), 2007447. https://doi.org/https://doi.org/10.1002/adfm.202007447.

(12) Li, P.; Dong, H.; Xu, J.; Chen, J.; Jiao, B.; Hou, X.; Li, J.; Wu, Z. Ligand Orientation-Induced Lattice Robustness for Highly Efficient and Stable Tin-Based Perovskite Solar Cells. *ACS Energy Lett.* **2020**, *5* (7), 2327–2334. https://doi.org/10.1021/acsenergylett.0c00960.

(13) Lee, S. J.; Shin, S. S.; Kim, Y. C.; Kim, D.; Ahn, T. K.; Noh, J. H.; Seo, J.; Seok, S. Il. Fabrication of Efficient Formamidinium Tin Iodide Perovskite Solar Cells through SnF 2 -Pyrazine Complex. *J. Am. Chem. Soc.* **2016**, *138* (12), 3974–3977. https://doi.org/10.1021/jacs.6b00142.

(14) Jokar, E.; Chien, C.-H.; Tsai, C.-M.; Fathi, A.; Diau, E. W.-G. Robust Tin-Based Perovskite Solar Cells with Hybrid Organic Cations to Attain Efficiency Approaching 10%. *Adv. Mater.* **2019**, *31* (2), 1804835. https://doi.org/10.1002/adma.201804835.

(15) Khadka, D. B.; Shirai, Y.; Yanagida, M.; Miyano, K. Attenuating the Defect Activities with a Rubidium Additive for Efficient and Stable Sn-Based Halide Perovskite Solar Cells. *J. Mater. Chem. C* **2020**, *8* (7), 2307–2313. https://doi.org/10.1039/C9TC06206H.

(16) Kim, H.; Lee, Y. H.; Lyu, T.; Yoo, J. H.; Park, T.; Oh, J. H. Boosting the Performance and Stability of Quasi-Two-Dimensional Tin-Based Perovskite Solar Cells Using the Formamidinium Thiocyanate Additive. *J. Mater. Chem. A* **2018**, *6* (37), 18173–18182. https://doi.org/10.1039/C8TA05916K.

(17) Lee, S. J.; Shin, S. S.; Im, J.; Ahn, T. K.; Noh, J. H.; Jeon, N. J.; Seok, S. Il; Seo, J. Reducing Carrier Density in Formamidinium Tin Perovskites and Its Beneficial Effects on Stability and Efficiency of Perovskite Solar Cells. *ACS Energy Lett.* **2018**, *3* (1), 46–53. https://doi.org/10.1021/acsenergylett.7b00976.

(18) Gao, W.; Ran, C.; Li, J.; Dong, H.; Jiao, B.; Zhang, L.; Lan, X.; Hou, X.; Wu, Z. Robust Stability of Efficient Lead-Free Formamidinium Tin Iodide Perovskite Solar Cells Realized by Structural Regulation. *J. Phys. Chem. Lett.* **2018**, *9* (24), 6999–7006. https://doi.org/10.1021/acs.jpclett.8b03194.

(19) Jokar, E.; Chien, C.-H.; Fathi, A.; Rameez, M.; Chang, Y.-H.; Diau, E. W.-G. Slow Surface Passivation and Crystal Relaxation with Additives to Improve Device Performance and Durability for Tin-Based Perovskite Solar Cells. *Energy Environ. Sci.* **2018**, *11* (9), 2353–2362. https://doi.org/10.1039/C8EE00956B.

(20) Shao, S.; Liu, J.; Portale, G.; Fang, H.-H.; Blake, G. R.; ten Brink, G. H.; Koster, L. J. A.; Loi, M. A. Highly Reproducible Sn-Based Hybrid Perovskite Solar Cells with 9% Efficiency. *Adv. Energy Mater.* **2018**, *8* (4), 1702019. https://doi.org/10.1002/aenm.201702019.

(21) Jiang, X.; Wang, F.; Wei, Q.; Li, H.; Shang, Y.; Zhou, W.; Wang, C.; Cheng, P.; Chen, Q.; Chen, L.; Ning, Z. Ultra-High Open-Circuit Voltage of Tin Perovskite Solar Cells via an Electron Transporting Layer Design. *Nat. Commun.* **2020**, *11* (1), 1245. https://doi.org/10.1038/s41467-020-15078-2.

(22) Kayesh, M. E.; Matsuishi, K.; Kaneko, R.; Kazaoui, S.; Lee, J.-J.; Noda, T.; Islam, A. Coadditive Engineering with 5-Ammonium Valeric Acid Iodide for Efficient and Stable Sn Perovskite Solar Cells. *ACS Energy Lett.* **2019**, *4* (1), 278–284. https://doi.org/10.1021/acsenergylett.8b02216.

(23) Nishimura, K.; Kamarudin, M. A.; Hirotani, D.; Hamada, K.; Shen, Q.; Iikubo, S.; Minemoto, T.; Yoshino, K.; Hayase, S. Lead-Free Tin-Halide Perovskite Solar Cells with 13% Efficiency. *Nano Energy* **2020**, *74*, 104858. https://doi.org/10.1016/j.nanoen.2020.104858.

(24) Liao, M.; Yu, B.-B.; Jin, Z.; Chen, W.; Zhu, Y.; Zhang, X.; Yao, W.; Duan, T.; Djerdj, I.; He, Z. Efficient and Stable FASnI3 Perovskite Solar Cells with Effective Interface Modulation by Low-Dimensional Perovskite Layer. *ChemSusChem* **2019**, *12* (22), 5007–5014. https://doi.org/10.1002/cssc.201902000.

(25) Wu, T.; Cui, D.; Liu, X.; Meng, X.; Wang, Y.; Noda, T.; Segawa, H.; Yang, X.; Zhang, Y.; Han, L. Efficient and Stable Tin Perovskite Solar Cells Enabled by Graded Heterostructure of Light-Absorbing Layer. *Sol. RRL* **2020**, *4* (9), 2000240. https://doi.org/10.1002/solr.202000240.

(26) Jokar, E.; Cheng, P.-Y.; Lin, C.-Y.; Narra, S.; Shahbazi, S.; Wei-Guang Diau, E. Enhanced Performance and Stability of 3D/2D Tin Perovskite Solar Cells Fabricated with a Sequential Solution Deposition. *ACS Energy Lett.* **2021**, *6* (2), 485–492. https://doi.org/10.1021/acsenergylett.0c02305.

(27) Jiang, X.; Li, H.; Zhou, Q.; Wei, Q.; Wei, M.; Jiang, L.; Wang, Z.; Peng, Z.; Wang, F.; Zang, Z.; Xu, K.; Hou, Y.; Teale, S.; Zhou, W.; Si, R.; Gao, X.; Sargent, E. H.; Ning, Z. One-Step Synthesis of SnI2·(DMSO)x Adducts for High-Performance Tin Perovskite Solar Cells. *J. Am. Chem. Soc.* **2021**, *143* (29), 10970–10976. https://doi.org/10.1021/jacs.1c03032.

(28) Xie, G.; Xu, L.; Sun, L.; Xiong, Y.; Wu, P.; Hu, B. Insight into the Reaction Mechanism of Water, Oxygen and Nitrogen Molecules on a Tin Iodine Perovskite Surface. *J. Mater. Chem. A* **2019**, *7* (10), 5779–5793. https://doi.org/10.1039/c8ta11705e.

(29) Numata, Y.; Sanehira, Y.; Ishikawa, R.; Shirai, H.; Miyasaka, T. Thiocyanate Containing Two-Dimensional Cesium Lead Iodide Perovskite, Cs 2 PbI 2 (SCN) 2 : Characterization, Photovoltaic Application, and Degradation Mechanism. *ACS Appl. Mater. Interfaces* **2018**, *10* (49), 42363–42371. https://doi.org/10.1021/acsami.8b15578.

(30) Kim, D.; Jung, H. J.; Park, I. J.; Larson, B. W.; Dunfield, S. P.; Xiao, C.; Kim, J.; Tong, J.; Boonmongkolras, P.; Ji, S. G.; Zhang, F.; Pae, S. R.; Kim, M.; Kang, S. B.; Dravid, V.; Berry, J. J.; Kim, J. Y.; Zhu, K.; Kim, D. H.; Shin, B. Efficient, Stable Silicon

Tandem Cells Enabled by Anion-Engineered Wide-Bandgap Perovskites. *Science* **2020**, *368* (6487), 155–160. https://doi.org/10.1126/science.aba3433.

(31) Xu, S.; Liu, G.; Zheng, H.; Xu, X.; Zhang, L.; Xu, H.; Zhu, L.; Kong, F.; Li, Y.; Pan, X. Boosting Photovoltaic Performance and Stability of Super-Halogen-Substituted Perovskite Solar Cells by Simultaneous Methylammonium Immobilization and Vacancy Compensation. *ACS Appl. Mater. Interfaces* **2020**, *12* (7), 8249–8259. https://doi.org/10.1021/acsami.9b21074.

(32) Kim, H.; Lee, J. W.; Han, G. R.; Kim, S. K.; Oh, J. H. Synergistic Effects of Cation and Anion in an Ionic Imidazolium Tetrafluoroborate Additive for Improving the Efficiency and Stability of Half-Mixed Pb-Sn Perovskite Solar Cells. *Adv. Funct. Mater.* **2021**, *31* (11), 2008801. https://doi.org/10.1002/adfm.202008801.

(33) Walker, B.; Kim, G.; Kim, J. Y. Pseudohalides in Lead-Based Perovskite Semiconductors. *Adv. Mater.* **2019**, *31* (20), 1807029. https://doi.org/10.1002/adma.201807029.

(34) Jeong, J.; Kim, M.; Seo, J.; Lu, H.; Ahlawat, P.; Mishra, A.; Yang, Y.; Hope, M. A.; Eickemeyer, F. T.; Kim, M.; Yoon, Y. J.; Choi, I. W.; Darwich, B. P.; Choi, S. J.; Jo, Y.; Lee, J. H.; Walker, B.; Zakeeruddin, S. M.; Emsley, L.; Rothlisberger, U.; Hagfeldt, A.; Kim, D. S.; Grätzel, M.; Kim, J. Y. Pseudo-Halide Anion Engineering for α-FAPbI3 Perovskite Solar Cells. *Nature* **2021**, *592* (7854), 381–385. https://doi.org/10.1038/s41586-021-03406-5.

(35) Zöller, T.; Iovkova-Berends, L.; Berends, T.; Dietz, C.; Bradtmöller, G.; Jurkschat, K. Intramolecular N→Sn Coordination in Tin(II) and Tin(IV) Compounds Based on Enantiopure Ephedrine Derivatives. *Inorg. Chem.* **2011**, *50* (17), 8645–8653. https://doi.org/10.1021/ic201203u.

(36) Meng, X.; Lin, J.; Liu, X.; He, X.; Wang, Y.; Noda, T.; Wu, T.; Yang, X.; Han, L. Highly Stable and Efficient FASnI 3 -Based Perovskite Solar Cells by Introducing Hydrogen Bonding. *Adv. Mater.* **2019**, *31* (42), 1903721. https://doi.org/10.1002/adma.201903721.

(37) Yang, S.; Liu, W.; Zuo, L.; Zhang, X.; Ye, T.; Chen, J.; Li, C.-Z.; Wu, G.; Chen, H. Thiocyanate Assisted Performance Enhancement of Formamidinium Based Planar Perovskite Solar Cells through a Single One-Step Solution Process. *J. Mater. Chem. A* **2016**, *4* (24), 9430–9436. https://doi.org/10.1039/C6TA02999J.

(38) Yu, B.; Shi, J.; Tan, S.; Cui, Y.; Zhao, W.; Wu, H.; Luo, Y.; Li, D.; Meng, Q. Efficient (>20%) and Stable All-Inorganic Cesium Lead Triiodide Solar Cell Enabled by Thiocyanate Molten Salts. *Angew. Chemie Int. Ed.* **2021**, *60* (24), 13436–13443. https://doi.org/10.1002/anie.202102466.

(39) Yu, Y.; Wang, C.; Grice, C. R.; Shrestha, N.; Zhao, D.; Liao, W.; Guan, L.; Awni, R. A.; Meng, W.; Cimaroli, A. J.; Zhu, K.; Ellingson, R. J.; Yan, Y. Synergistic Effects of Lead Thiocyanate Additive and Solvent Annealing on the Performance of Wide-Bandgap Perovskite Solar Cells. *ACS Energy Lett.* **2017**, *2* (5), 1177–1182. https://doi.org/10.1021/acsenergylett.7b00278.

(40) Tong, J.; Song, Z.; Kim, D. H.; Chen, X.; Chen, C.; Palmstrom, A. F.; Ndione, P. F.; Reese, M. O.; Dunfield, S. P.; Reid, O. G.; Liu, J.; Zhang, F.; Harvey, S. P.; Li, Z.; Christensen, S. T.; Teeter, G.; Zhao, D.; Al-Jassim, M. M.; van Hest, M. F. A. M.; Beard, M. C.; Shaheen, S. E.; Berry, J. J.; Yan, Y.; Zhu, K. Carrier Lifetimes of >1 Ms in Sn-Pb Perovskites Enable Efficient All-Perovskite Tandem Solar Cells. *Science* **2019**, *364* (6439), 475–479. https://doi.org/10.1126/science.aav7911.

(41) Rameez, M.; Shahbazi, S.; Raghunath, P.; Lin, M. C.; Hung, C. H.; Diau, E. W.-G. Development of Novel Mixed Halide/Superhalide Tin-Based Perovskites for Mesoscopic Carbon-Based Solar Cells. *J. Phys. Chem. Lett.* **2020**, *11* (7), 2443–2448. https://doi.org/10.1021/acs.jpclett.0c00479.

(42) Rameez, M.; Lin, E. Y.-R.; Raghunath, P.; Narra, S.; Song, D.; Lin, M.-C.; Hung, C.-H.; Diau, E. W.-G. Development of Hybrid Pseudohalide Tin Perovskites for Highly Stable Carbon-Electrode Solar Cells. *ACS Appl. Mater. Interfaces* **2020**, *12* (19), 21739–21747. https://doi.org/10.1021/acsami.0c03704.

(43) Chen, Y.; Li, B.; Huang, W.; Gao, D.; Liang, Z. Efficient and Reproducible CH3NH3PbI3-x(SCN)x Perovskite Based Planar Solar Cells. *Chem. Commun.* **2015**, *51* (60), 11997–11999. https://doi.org/10.1039/c5cc03615a.

(44) Lian, X.; Chen, J.; Zhang, Y.; Qin, M.; Li, J.; Tian, S.; Yang, W.; Lu, X.; Wu, G.; Chen, H. Highly Efficient Sn/Pb Binary Perovskite Solar Cell via Precursor Engineering: A Two-Step Fabrication Process. *Adv. Funct. Mater.* **2019**, *29* (5), 1807024. https://doi.org/10.1002/adfm.201807024.

(45) Jiang, Q.; Rebollar, D.; Gong, J.; Piacentino, E. L.; Zheng, C.; Xu, T. Pseudohalide-

Induced Moisture Tolerance in Perovskite CH 3 NH 3 Pb(SCN) 2 I Thin Films. *Angew. Chemie Int. Ed.* **2015**, *54* (26), 7617–7620. https://doi.org/10.1002/anie.201503038.

(46) Min, H.; Kim, M.; Lee, S.-U.; Kim, H.; Kim, G.; Choi, K.; Lee, J. H.; Seok, S. Il. Efficient, Stable Solar Cells by Using Inherent Bandgap of α-Phase Formamidinium Lead Iodide. *Science* **2019**, *366* (6466), 749–753. https://doi.org/10.1126/science.aay7044.

(47) Zhang, H.; Hou, M.; Xia, Y.; Wei, Q.; Wang, Z.; Cheng, Y.; Chen, Y.; Huang, W. Synergistic Effect of Anions and Cations in Additives for Highly Efficient and Stable Perovskite Solar Cells. *J. Mater. Chem. A* **2018**, *6* (19), 9264–9270. https://doi.org/10.1039/C8TA00308D.

(48) Wang, C.; Gu, F.; Zhao, Z.; Rao, H.; Qiu, Y.; Cai, Z.; Zhan, G.; Li, X.; Sun, B.; Yu, X.; Zhao, B.; Liu, Z.; Bian, Z.; Huang, C. Self-Repairing Tin-Based Perovskite Solar Cells with a Breakthrough Efficiency Over 11%. *Adv. Mater.* **2020**, *32* (31), 1907623. https://doi.org/10.1002/adma.201907623.

(49) Wang, F.; Jiang, X.; Chen, H.; Shang, Y.; Liu, H.; Wei, J.; Zhou, W.; He, H.; Liu, W.; Ning, Z. 2D-Quasi-2D-3D Hierarchy Structure for Tin Perovskite Solar Cells with Enhanced Efficiency and Stability. *Joule* **2018**, *2* (12), 2732–2743. https://doi.org/10.1016/j.joule.2018.09.012.

(50) Li, F.; Pei, Y.; Xiao, F.; Zeng, T.; Yang, Z.; Xu, J.; Sun, J.; Peng, B.; Liu, M. Tailored Dimensionality to Regulate the Phase Stability of Inorganic Cesium Lead Iodide Perovskites. *Nanoscale* **2018**, *10* (14), 6318–6322. https://doi.org/10.1039/C8NR00758F.

(51) Nakane, A.; Tampo, H.; Tamakoshi, M.; Fujimoto, S.; Kim, K. M.; Kim, S.; Shibata, H.; Niki, S.; Fujiwara, H. Quantitative Determination of Optical and Recombination Losses in Thin-Film Photovoltaic Devices Based on External Quantum Efficiency Analysis. *J. Appl. Phys.* **2016**, *120* (6), 064505. https://doi.org/10.1063/1.4960698.

(52) Zhang, J.; Wu, S.; Liu, T.; Zhu, Z.; Jen, A. K. Y. Boosting Photovoltaic Performance for Lead Halide Perovskites Solar Cells with BF4-Anion Substitutions. *Adv. Funct. Mater.* **2019**, *29* (47), 1808833. https://doi.org/10.1002/adfm.201808833.

(53) Turren-Cruz, S.-H.; Saliba, M.; Mayer, M. T.; Juárez-Santiesteban, H.; Mathew, X.;

Nienhaus, L.; Tress, W.; Erodici, M. P.; Sher, M.-J.; Bawendi, M. G.; Grätzel, M.; Abate, A.; Hagfeldt, A.; Correa-Baena, J.-P. Enhanced Charge Carrier Mobility and Lifetime Suppress Hysteresis and Improve Efficiency in Planar Perovskite Solar Cells. *Energy Environ. Sci.* **2018**, *11* (1), 78–86. https://doi.org/10.1039/C7EE02901B.

(54) Khadka, D. B.; Shirai, Y.; Yanagida, M.; Miyano, K. Unraveling the Impacts Induced by Organic and Inorganic Hole Transport Layers in Inverted Halide Perovskite Solar Cells. *ACS Appl. Mater. Interfaces* **2019**, *11* (7), 7055–7065. https://doi.org/10.1021/acsami.8b20924.

(55) Warren, C. W.; Roe, E. T.; Miller, D. W.; Shafarman, W. N.; Lonergan, M. C. An Improved Method for Determining Carrier Densities via Drive Level Capacitance Profiling. *Appl. Phys. Lett.* **2017**, *110* (20), 203901. https://doi.org/10.1063/1.4983367.

(56) Miyano, K.; Yanagida, M.; Shirai, Y. Impedance Spectroscopy Revisited. *Adv. Energy Mater.* **2020**, *10* (26), 1903097. https://doi.org/10.1002/aenm.201903097.

(57) Eames, C.; Frost, J. M.; Barnes, P. R. F.; O'Regan, B. C.; Walsh, A.; Islam, M. S. Ionic Transport in Hybrid Lead Iodide Perovskite Solar Cells. *Nat. Commun.* **2015**, *6* (1), 7497. https://doi.org/10.1038/ncomms8497.

(58) Khadka, D. B.; Shirai, Y.; Yanagida, M.; Masuda, T.; Miyano, K. Enhancement in Efficiency and Optoelectronic Quality of Perovskite Thin Films Annealed in MACl Vapor. *Sustain. Energy Fuels* **2017**, *1* (4), 755–766. https://doi.org/10.1039/C7SE00033B.

Table of Content Graphics

The organic cations with pseudohalide derivative as PEASCN additive in $FASnI_3$ film improved the device efficiency and stability as a consequence of the reduction of the extent of Sn^{2+} oxidation and alleviation of defect characteristics.